Regulation of Solvation Structure and electrode Interface by Succinic Acid Additive for Highly Stable Aqueous Zn Batteries

Yuanjun Zhang,[a,1] Fangfang Yu,[b,1] Haoxuan Liu,[b] Nana Wang,[b] Xianzhong Yang,[c] Shunjian Xu,[a] Chao Wu,[b,c,*] Hua-Kun Liu,[b,c] and Shi-Xue Dou[b,c,*]

[a]Huzhou Key Laboratory of Green Energy Materials and Battery Cascade Utilization，School of Intelligent Manufacturing, Huzhou College, Huzhou, 313000, China.

[b]Institute for Superconducting & Electronic Materials, Australian Institute of Innovative Materials, University of Wollongong, NSW 2522, Australia

[c]Institute of Energy Materials Science (IEMS), University of Shanghai for Science and Technology, Shanghai 200093, China

[1]These two authors (Y. Zhang and F. Yu) contributed equally to this work.

Email: chaowu@uow.edu.au; shi@uow.edu.au

Materials and methods

Materials

For the prepration of aqueous elelctrolytes, all of the raw materials were already commercially sourced. Succinic acid (SA) and $ZnSO_4 \cdot 7H_2O$ were purchased from Adamas (Tansoole, China). Stainless steel (SS) and Zn foil (thicknesses of 50 μm and 10 μm) were supplied by Canrd (China). Cu foil was purchased from DodoChem.

Preparation of aqueous electrolytes

A 2 m aqueous electrolyte of $ZnSO_4$ was prepared by dissolving a specific amount of $ZnSO_4$ into the deionized water. Aqueous electrolyte containing 2 m $ZnSO_4$ and 0.1 m SA was prepared by dissolving a specific amount of SA into the aforementioned electrolyte.

Synthesis of $K_{0.27}MnO_2 \cdot 0.54H_2O$ cathodes materials

The synthesis of $K_{0.27}MnO_2 \cdot 0.54H_2O$ (KMnO) referred to the previous work.[1]

Electrochemical measurements

The corrosion experiments were performed on an electrochemical workstation (Autolab). Zn foil served as both the counter and working electrodes in the corrosion test, and saturated calomel electrode (SCE) served as the reference electrode. The electrochemical performances of Zn plating/stripping were assessed in CR2032 coin cells. To evaluate Coulombic efficiency, the Cu foil functioned as the working electrode, while the Zn foil acted as the counter electrode, and a disk-shaped piece of glass fiber paper served as the separator. In the Zn||Zn symmetric cell, the disk-shaped Zn foils were utilized as the electrodes. The KMnO cathodes were constructed by casting a slurry of binder (PVDF), super P, and KMnO with a mass ratio of 10:20:70 onto a stainless steel foil. The cathodes was then vacuum-dried at 80 °C before being cut into 10 mm-diameter disk-shaped sheets. The full cells were then assembled with KMnO as cathodes, using an aqueous electrolyte with/without SA and a 50 μm Zn metal anode. All samples were tested for their electrochemical performance at room temperature using a LANHE battery tester (CT2001A, Wuhan LAND electronics Co., Ltd., China).

The exchange current density (i_0) of the zinc plating/stripping process was calculated based on the charge/discharge profiles of zinc-based symmetric cells and equation:

$$i = i_0 \frac{F}{RT} \cdot \frac{\eta}{2}$$

in which F is the Faraday's constant and η is the total overpotential of charge/discharge profiles. The Arrhenius equation was used to determine the activation energy (E_a) of the zinc deposition process, as follows:

$$\frac{1}{R_{ct}} = Aexp\left(-\frac{E_0}{RT}\right)$$

where R_{ct}, A, R and T represent the charge transfer resistance at various temperatures, the frequency factor, the gas constant and the absolute temperature, respectively.[2, 3]

Material characterizations

X-ray diffraction (XRD, Rigaku D/MAX2200V PC) was used to record the crystal structures of the samples. Scanning electron microscopy (SEM, JEOL 7500F) was utilized to examine the Zn metal anode morphologies. A special device supplied by Beijing Science Star Technology Co. Ltd. was employed to conduct *in-situ* optical microscopy observations.

Models and computational details

In this study, the following functional form was employed with a standard molecular mechanic's potential model:

$$u(r^N) = \sum_{bonds} \frac{k_i}{2}(l_i - l_{i,0})^2 + \sum_{angles} \frac{k_i}{2}(\theta_i - \theta_{i,0})^2 + \sum_{torsions} \frac{V_n}{2}(1 + \cos(n\omega - \gamma))$$

$$+ \sum_{i=1}^{N} \sum_{j=i+1}^{N} \left(4\varepsilon_{ij} \left[\left(\frac{\sigma_{ij}}{r_{ij}} \right)^{12} - \left(\frac{\sigma_{ij}}{r_{ij}} \right)^{6} \right] + \frac{q_i q_j}{r_{ij}} \right)$$

where the initial three terms represent bonded interactions including angle, bond, and torsion. The second terms represent nonbonded interactions, such as Coulombic interactions and van der Waals (vdW). The Lorentz-Berthelot mix rules were selected for vdW interactions for various types of atoms, and they are given in the following equation:

$$\sigma_{ij} = \frac{1}{2}(\sigma_{ii} + \sigma_{jj});\ \varepsilon_{ij} = (\varepsilon_{ii} * \varepsilon_{jj})^{1/2}$$

Two systems were developed in accordance with the experimental conditions. Systems were designed with their initial configurations using the Packmol software [4]. The simulations were carried out with the GROMACS (version 2019.3) software [5-8] and the all-atom OPLS (optimized performance for liquid systems) force field [9]. The steep descent strategy was applied to each system to reduce system energy. After that, 10 ns of molecular dynamics simulations were conducted for each system under the NPT ensemble at 298 K and 1 atm to obtain trajectories for the following data analysis. Other components' bond lengths were constrained using the LINCS algorithm [10]. All three directions were subjected to periodic boundary conditions. By employing the V-rescale thermostat algorithm, the temperature was kept constant[11]. Electrostatic interactions and Lennard-Jones had a 1.2 nm cutoff distance. The electrostatic interactions at a long distance were calculated using the particle mesh Ewald approach[12]. The software Visual Molecular Dynamics [13] was employed to visualize the configurations.

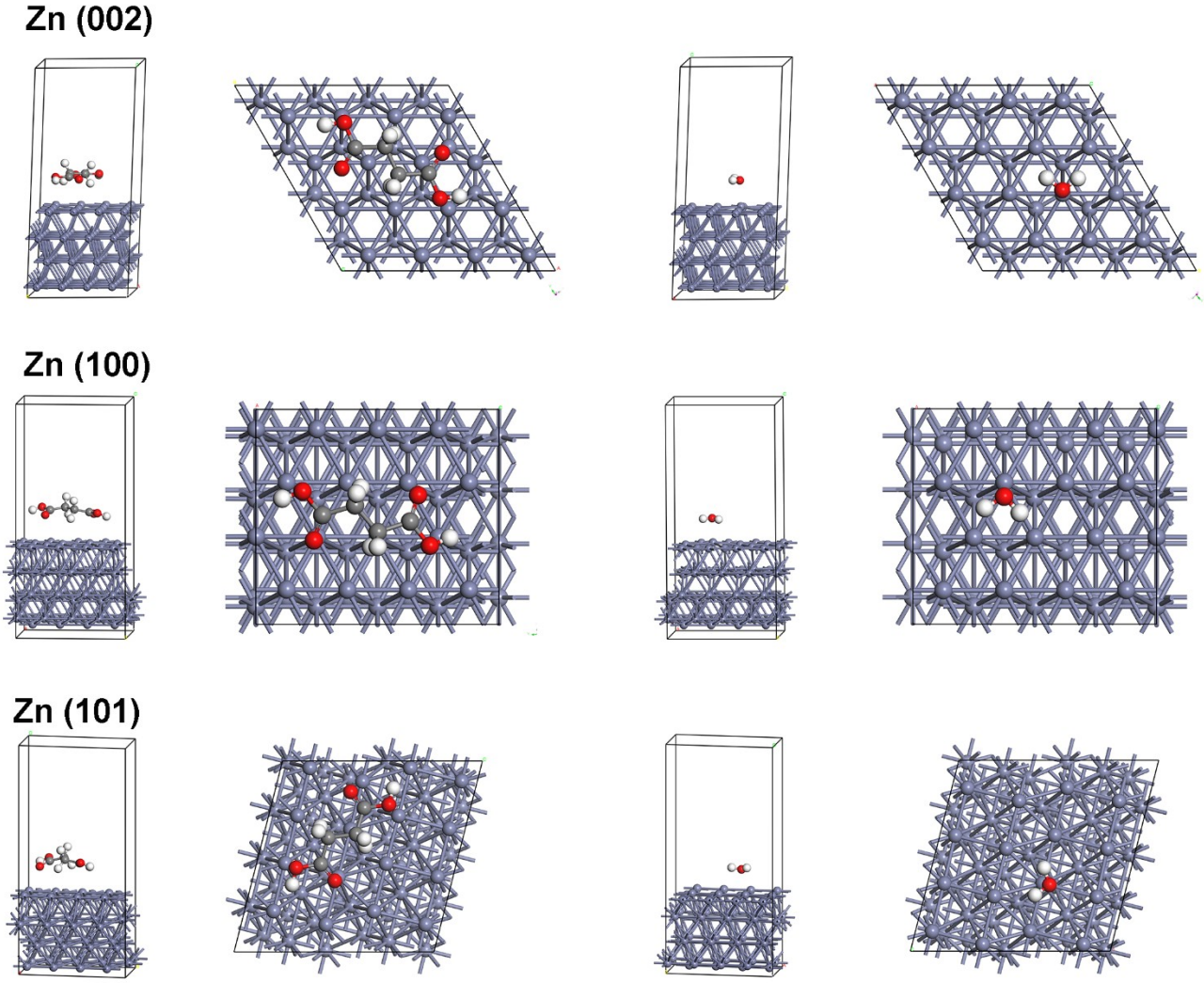

Figure. S1 Corresponding computational models for binding energy.

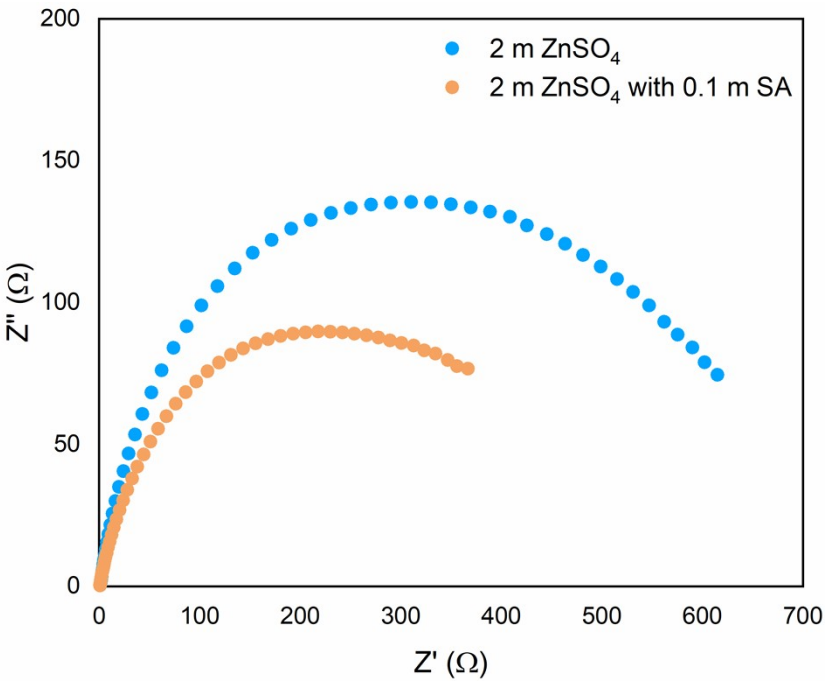

Figure. S2 EIS of Zn||Zn symmetric cells in the 2 m $ZnSO_4$ with 0.1 m SA and 2 m $ZnSO_4$ electrolyte.

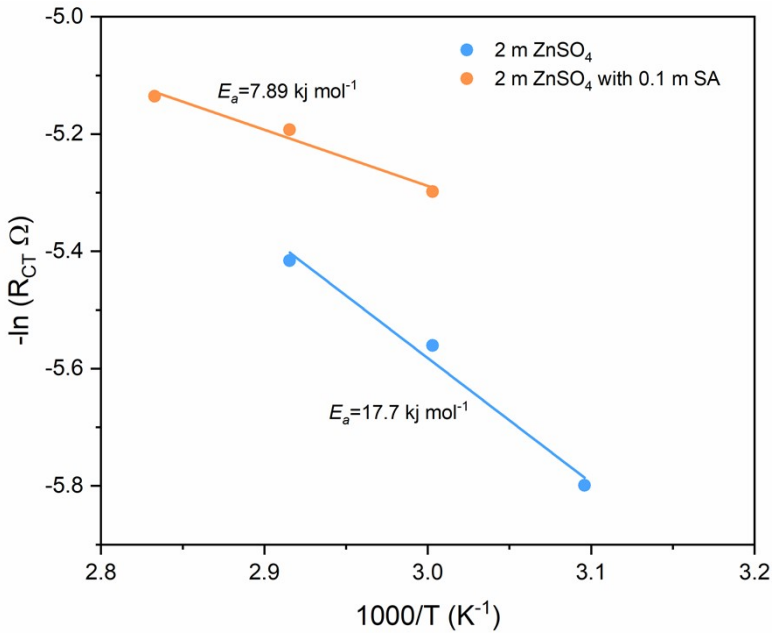

Figure. S3 Zn deposition activation energy.

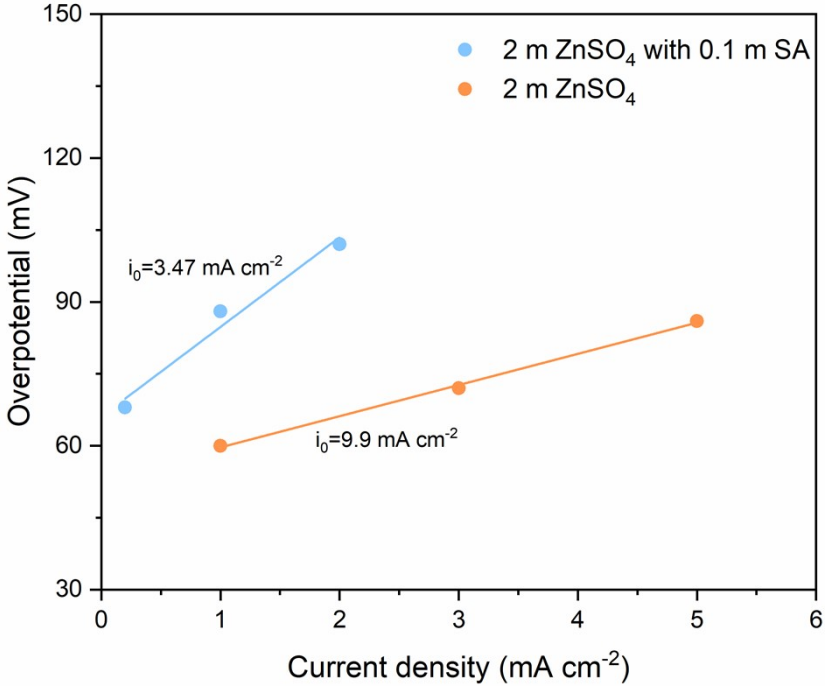

Figure. S4 Exchange current calculation of Zn based symmetric cells in 2 m $ZnSO_4$ with 0.1 m SA and 2 m $ZnSO_4$ electrolytes at diverse current densities.

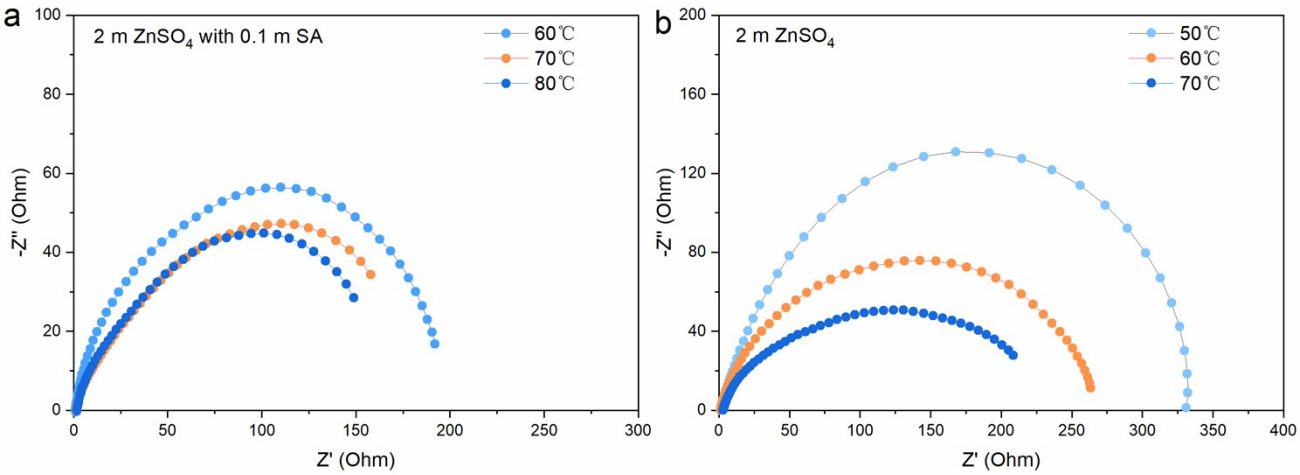

Figure. S5 EIS spectra of symmetric cells at different temperatures.

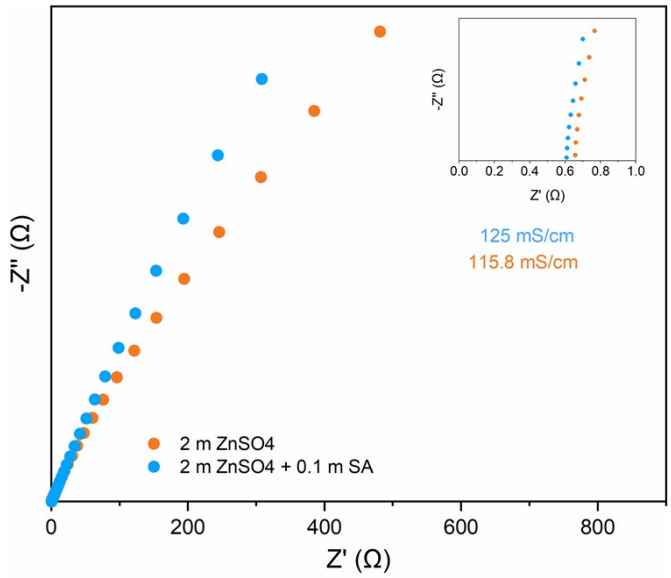

Figure. S6 Ionic conductivities and SS||SS coin cell electrochemical impedance spectra.

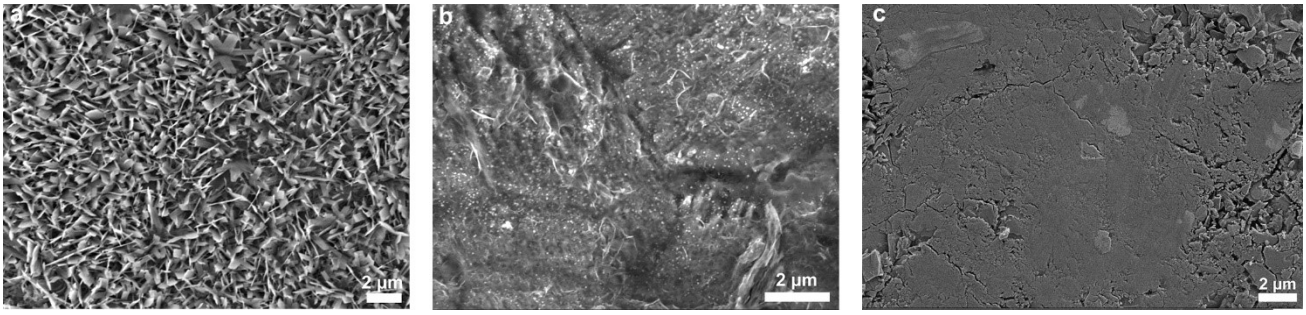

Figure. S7 (a-b) SEM images of the Zn electrode after cycling for (a) 10 h in an electrolyte of 2 m $ZnSO_4$; (b) 10 h and (c) 200 h in an electrolyte of 2 m $ZnSO_4$ with 0.1 m SA at 1 mAh cm^{-2}/1 mA cm^{-2}.

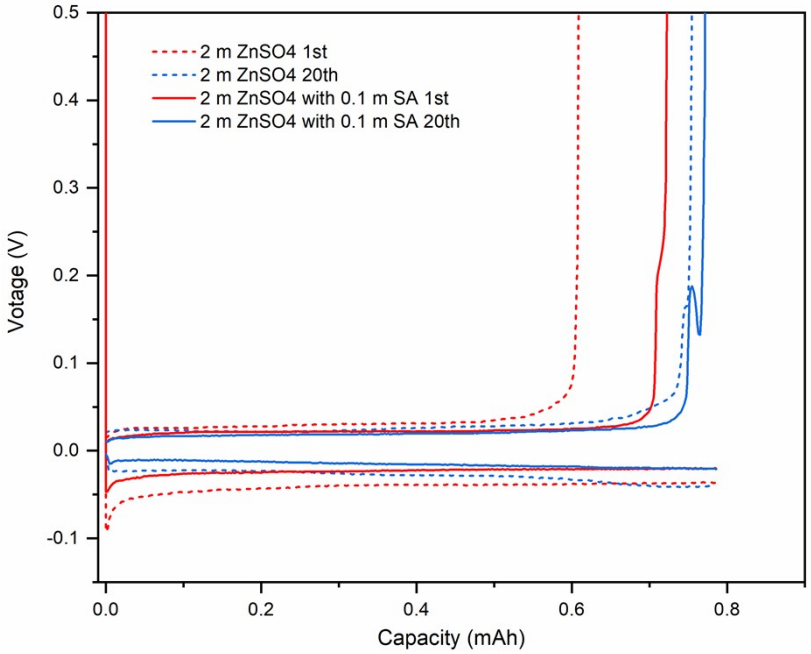

Figure. S8 Voltage profiles of Zn plating/stripping on Cu foil at 1 mA cm^{-2}/1 mAh cm^{-2}.

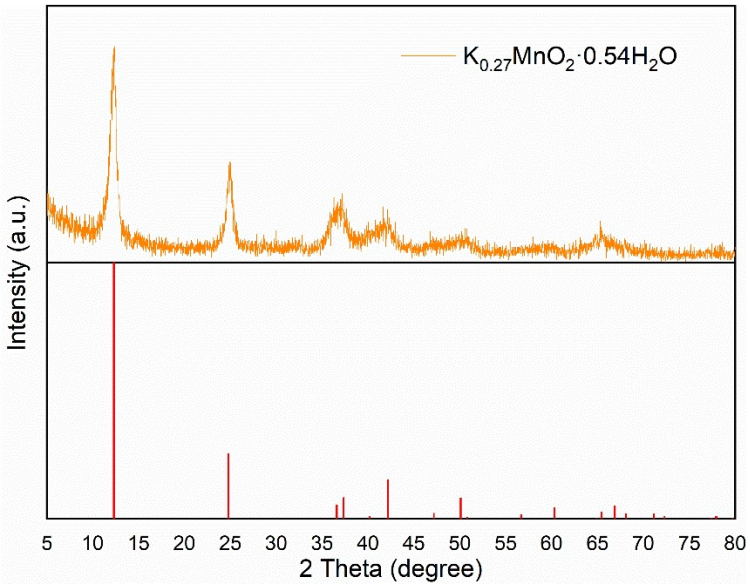

Figure. S9 XRD patterns of $K_{0.27}MnO_2 \cdot 0.54H_2O$.

Table S1 The performance comparison of the symmetric Zn||Zn cells available through the modified strategies.

No.	Strategies	Current density ($mA\ cm^{-2}$)	Capacity ($mAh\ cm^{-2}$)	Cycle time (h)	References
1	$ZnSiO_3$@Zn	1	1	1600	[1]
2	$ZnSO_4$ + cysteine	5	5	650	[14]
3	$ZnSO_4$ + aromatic aldehyde	1	1	3000	[15]
		5	5	800	
4	3D-COOH-COF@Zn	1	1	2000	[16]
5	Sn-PCF@Zn	1	1	750	[17]
6	0.5 M $ZnSO_4$ + 0.1 mM TBA_2SO_4	5	5	160	[18]
7	ZIF-8-modified Zn	5	5	400	[19]
8	graphene-modified glass fiber separator	5	5	75	[20]
9	$ZnSO_4$ + La $(NO_3)_3$	1	1	1200	[21]
10	□Negatively charged porous layer@Zn	5	5	300	[22]
11	Zn (002)	5	5	200	[23]
12	$ZnSO_4$ + N, N-Dimethylacetamide	1	1	1900	[24]
13	2 M $ZnSO_4$ + glucose	5	5	270	[25]
14	Zn@MXene@Sb	5	5	550	[26]
15	BIS-TRIS additive	5	5	650	[27]
16	P(AA-co-AMPS)-MXene @ Zn	1	1	950	[28]
17	COP-CMC-Zn	5	3	2000	[29]
18	$ZnSO_4$ + α-CD	5	5	200	[30]
19	Sn-coated cellulose separator	5	5	1000	[31]
20	Si_3N_4@Zn	5	5	800	[32]
21	CaF_2@Zn	1	1	750	[33]
22	weighing paper	1	1	2400	[34]
23	S/MX@ZnS@Zn	5	5	400	[35]
24	$Ti_3C_2T_x$ MXene-decorated Janus separator	1	1	1200	[36]
25	Nettle extract (NE) additive	5	5	2200	[37]
26	$ZnSO_4$ + sodium hyaluronate	1	1	5000	[38]
27	DMF electrolyte	5	5	1450	[39]
28	MTSi-Hedp@Zn	1	1	1250	[40]
29	benzyltrimethylammonium chloride additive	5	5	550	[41]
30	$ZnCl_2$/EG	1	1	3200	[42]
31	$ZnSO_4$ + Ch^+	1	1	2000	[43]
32	polyanthraquinone@Zn	1	1	1750	[44]
33	ROZ@Zn	1	1	1250	[45]

34	Zn_3Hg	1	1	2000	[46]
35	ovalent triazine framework@Zn	1	1	900	[47]
36	silk fibroin additives	1	1	1600	[48]
37	oleic acid additives	1	1	3400	[49]
38	polyamino acid additives	1	1	2100	[50]
39	**$ZnSO_4$ + SA**	**1**	**1**	**5500**	**This work**
		5	**5**	**1500**	

Table S2 The performance comparison of the symmetric cells with high DOD available through the modified strategies.

No.	Strategies	DOD (%)	Cycle time (h)	References
1	N, S-doped carbon quantum dots (NSQDs) electrolyte additive	50	145	[51]
2	Zn(DBS)2 as Zn salt in a mixture of acetamide and water.	50	600	[52]
3	(002)-textured	45.5	220	[53]
4	Cyclic tetramethylene sulfone electrolyte additive	26	250	[54]
5	texture the Zn electrodeposits	37..5	190	[55]
6	xylitol-based electrolyte	28.5	450	[56]
		56.9	100	
7	Versatile 1, 3-dimethyl-2-imidazolidinone electrolyte additive:	17.112	125	[57]
8	lithium acetate (LiOAc) electrolyte additive	20	600	[58]
9	Zn(BF4)2 electrolyte additive	51.3	360	[59]
10	ZnMoO4@Zn	50	625	[60]
11	GF Janus separator	56	220	[61]
12	thiourea electrolyte additive	20	140	[62]
13	Zn@CNF	40	380	[63]
14	Theophylline electrolyte additive	40	650	[64]
15	maltose electrolyte additive	17.1	600	[65]
16		51.3	240	
17	zinc-titanium alloy	25	120	[66]
18	$ZnSO_4$ + SA	51	650	This work

Reference

[1] Guo R., Liu X., Xia F., Jiang Y., Zhang H., Huang M., Niu C., Wu J., Zhao Y., Wang X., Han C.., Mai L., Large-Scale Integration of Zinc Metasilicate Interface Layer Guiding Well-Regulated Zn Deposition. *Adv. Mater.* **2022**, *34*, e2202188.

[2] Li Y., Peng X., Li X., Duan H., Xie S., Dong L.., Kang F., Functional Ultrathin Separators Proactively Stabilizing Zinc Anodes for Zinc-Based Energy Storage. *Adv. Mater.* **2023**, *35*, e2300019.

[3] Zheng Z., Ren D., Li Y., Kang F., Li X., Peng X.., Dong L., Self‐Assembled Robust Interfacial Layer for Dendrite‐Free and Flexible Zinc‐Based Energy Storage. *Adv. Funct. Mater.* **2024**. https://doi.org/10.1002/adfm.202312855.

[4] Martínez L., Andrade R., Birgin E. G.., Martínez J. M., Packmol: A package for building initial configurations for molecular dynamics simulations. *J Comput Chem* **2009**, *30*, 2157-2164.

[5] Abraham M. J., Murtola T., Schulz R., Páll S., Smith J. C., Hess B.., Lindahl E., GROMACS: High performance molecular simulations through multi-level parallelism from laptops to supercomputers. *SoftwareX* **2015**, *6*, 19–25.

[6] Páll S., Abraham M. J., Kutzner C., Hess B.., Lindahl E., Tackling exascale software challenges in molecular dynamics simulations with GROMACS. *Solving Software Challenges for Exascale* **2015**, *8759*, 3–27.

[7] Pronk S., Páll S., Schulz R.., Larsson P., GROMACS 4.5: a high-throughput and highly parallel open source molecular simulation toolkit. *Bioinformatics* **2013**, *29*, 845–854.

[8] Hess B., Kutzner C., Spoel D. v. d.., Lindahl E., GROMACS 4: Algorithms for highly efficient, load-balanced, and scalable molecular simulation. *J. Chem. Theory. Comput* **2008**, *4*, 435–447.

[9] Jorgensen W. L., Maxwell D. S.., Tirado-Rives J., Development and Testing of the OPLS All-Atom Force Field on Conformational Energetics and Properties of Organic Liquids. *J. Am. Chem. Soc.* **1996**, *118*, 11225–11236.

[10] Hess B., Bekker H., Berendsen H. J. C.., Fraaije J. G. E. M., LINCS: A linear constraint solver for molecular simulations. *J. Comput. Chem.* **1997**, *18*, 1463–1472.

[11] Bussi G., Donadio D.., Parrinello M., Canonical sampling through velocity rescaling. *J. Phys. Chem.* **2007**, *126*, 014101.

[12] Essmann U., Perera L.., Berkowitz M. L., A smooth particle mesh Ewald method. *J. Phys. Chem.* **1995**, *103*, 8577–8593.

[13] Humphrey W., Dalke A.., Schulten K., VMD: Visual molecular dynamics. *J. Mol. Graph* **1996**, *14*, 33–38.

[14] Meng Q., Zhao R., Cao P., Bai Q., Tang J., Liu G., Zhou X.., Yang J., Stabilization of Zn anode via a multifunctional cysteine additive. *Chem. Eng. J.* **2022**, *447*, 137471.

[15] Qiu M., Ma L., Sun P., Wang Z., Cui G.., Mai W., Manipulating Interfacial Stability Via Absorption-Competition Mechanism for Long-Lifespan Zn Anode. *Nanomicro Lett* **2021**, *14*, 31.

[16] Wu K., Shi X., Yu F., Liu H., Zhang Y., Wu M., Liu H.-K., Dou S.-X., Wang Y.., Wu C., Molecularly engineered three-dimensional covalent organic framework protection films for highly stable zinc anodes in aqueous electrolyte. *Energy Stor. Mater.* **2022**, *51*, 391-399.

[17] Yang J.-L., Yang P., Yan W., Zhao J.-W.., Fan H. J., 3D zincophilic micro-scaffold enables stable Zn deposition. *Energy Stor. Mater.* **2022**, *51*, 259-265.

[18] Bayaguud A., Luo X., Fu Y.., Zhu C., Cationic Surfactant-Type Electrolyte Additive Enables Three-Dimensional Dendrite-Free Zinc Anode for Stable Zinc-Ion Batteries. *ACS Energy Lett.* **2020**, *5*, 3012-3020.

[19] Yuksel R., Buyukcakir O., Seong W. K.., Ruoff R. S., Metal-Organic Framework Integrated Anodes for Aqueous Zinc-Ion Batteries. *Adv. Energy Mater.* **2020**, *10*, 1904215.

[20] Li C., Sun Z., Yang T., Yu L., Wei N., Tian Z., Cai J., Lv J., Shao Y., Rümmeli M. H., Sun J.., Liu Z., Directly Grown Vertical Graphene Carpets as Janus Separators toward Stabilized Zn Metal Anodes. *Adv. Mater.* **2020**, *32*, 2003425.

[21] Zhao R., Wang H., Du H., Yang Y., Gao Z., Qie L.., Huang Y., Lanthanum nitrate as aqueous electrolyte additive for favourable zinc metal electrodeposition. *Nat. Commun.* **2022**, *13*, 3252.

[22] Kim S., Heo J., Kim R., Lee J. H., Seo J., Yoon S., Lee H., Kim S. J.., Kim H. T., Electrokinetic-Driven Fast Ion Delivery for Reversible Aqueous Zinc Metal Batteries with High Capacity. *Small.* **2021**, *17*, 2008059.

[23] Zhou M., Guo S., Li J., Luo X., Liu Z., Zhang T., Cao X., Long M., Lu B., Pan A., Fang G., Zhou J.., Liang S., Surface-Preferred Crystal Plane for a Stable and Reversible Zinc Anode. *Adv. Mater.* **2021**, *33*, e2100187.

[24] Wu F., Chen Y., Chen Y., Yin R., Feng Y., Zheng D., Xu X., Shi W., Liu W.., Cao X., Achieving Highly Reversible Zinc Anodes via N, N-Dimethylacetamide Enabled Zn-Ion Solvation Regulation. *Small.* **2022**, *18*, e2202363.

[25] Sun P., Ma L., Zhou W., Qiu M., Wang Z., Chao D.., Mai W., Simultaneous Regulation on Solvation Shell and Electrode Interface for Dendrite‐Free Zn Ion Batteries: Achieved by a Low‐Cost Glucose Additive. *Angew. Chem. Int. Ed.* **2021**, *60*, 18247-18255.

[26] Tian Y., An Y., Liu C., Xiong S., Feng J.., Qian Y., Reversible Zinc-Based Anodes Enabled by Zincophilic Antimony Engineered MXene for Stable and Dendrite-Free Aqueous Zinc Batteries. *Energy Stor. Mater.* **2021**, *41*, 343-353.

[27] Luo M., Wang C., Lu H., Lu Y., Xu B. B., Sun W., Pan H., Yan M.., Jiang Y., Dendrite-free zinc anode enabled by zinc-chelating chemistry. *Energy Stor. Mater.* **2021**, *41*, 515-521.

[28] Wang N., Wu Z., Long Y., Chen D., Geng C., Liu X., Han D., Zhang J., Tao Y.., Yang Q.-H., MXene-assisted polymer coating from aqueous monomer solution towards dendrite-free zinc anodes. *J. Energy Chem.* **2022**, *73*, 277-284.

[29] Ding J., Liu Y., Huang S., Wang X., Yang J., Wang L., Xue M., Zhang X.., Chen J., In Situ Construction of a Multifunctional Quasi-Gel Layer for Long-Life Aqueous Zinc Metal Anodes. *ACS Appl. Mater. Interfaces.* **2021**, *13*, 29746–29754.

[30] Zhao K., Fan G., Liu J., Liu F., Li J., Zhou X., Ni Y., Yu M., Zhang Y. M., Su H., Liu Q.., Cheng F., Boosting the Kinetics and Stability of Zn Anodes in Aqueous Electrolytes with Supramolecular Cyclodextrin Additives. *J. Am. Chem. Soc.* **2022**, *144*, 11129–11137.

[31] Hou Z., Gao Y., Tan H.., Zhang B., Realizing high-power and high-capacity zinc/sodium metal anodes through interfacial chemistry regulation. *Nat. Commun.* **2021**, *12*, 3083.

[32] Zhou S., Wang Y., Lu H., Zhang Y., Fu C., Usman I., Liu Z., Feng M., Fang G., Cao X., Liang S.., Pan A., Anti‐Corrosive and Zn‐Ion‐Regulating Composite Interlayer Enabling Long‐Life Zn Metal Anodes. *Adv. Funct. Mater.* **2021**, *31*, 2104361.

[33] Li Y., Yang S., Du H., Liu Y., Wu X., Yin C., Wang D., Wu X.-M., He Z.., Wu X., A Stable Fluoride-Based Interphase for Long Cycle Zn Metal Anode in Aqueous Zinc Ion Batteries. *J. Mater. Chem. A.* **2022**, *10*, 14399-14410.

[34] Guo Y., Cai W., Lin Y., Zhang Y., Luo S., Huang K., Wu H.., Zhang Y., An ion redistributor enabled by cost-effective weighing paper interlayer for dendrite free aqueous zinc-ion battery. *Energy Stor. Mater.* **2022**, *50*, 580-588.

[35] An Y., Tian Y., Liu C., Xiong S., Feng J.., Qian Y., Rational Design of Sulfur-Doped Three-Dimensional $Ti_3C_2T_x$ MXene/ZnS Heterostructure as Multifunctional Protective Layer for Dendrite-Free Zinc-Ion Batteries. *ACS nano.* **2021**, *15*, 15259–15273.

[36] Su Y., Liu B., Zhang Q., Peng J., Wei C., Li S., Li W., Xue Z., Yang X.., Sun J., Printing‐Scalable $Ti_3C_2T_x$ MXene‐Decorated Janus Separator with Expedited Zn^{2+} Flux toward Stabilized Zn Anodes. *Adv. Funct. Mater.* **2022**, *32*, 2204306.

[37] Zhang L., Miao L., Xin W., Peng H., Yan Z.., Zhu Z., Engineering zincophilic sites on Zn surface via plant extract additives for dendrite-free Zn anode. *Energy Stor. Mater.* **2021**, *44*, 408-415.

[38] Li Y., Wang Y., Xu Y., Tian W., Wang J., Cheng L., Yue H., Ji R., Zhu Q., Yuan H.., Wang H., Dynamic Biomolecular “Mask” Stabilizes Zn Anode. *Small.* **2022**, *18*, 2202214.

[39] Raza B., Naveed A., chen J., Lu H., Rasheed T., Yang J., NuLi Y.., Wang J., Zn anode sustaining high rate and high loading in organic electrolyte for rechargeable batteries. *Energy Stor. Mater.* **2022**, *46*, 523-534.

[40] Yu H., Chen Y., Wang H., Ni X., Wei W., Ji X.., Chen L., Engineering multi-functionalized molecular skeleton layer for dendrite-free and durable zinc batteries. *Nano Energy.* **2022**, *99*.

[41] Guan K., Tao L., Yang R., Zhang H., Wang N., Wan H., Cui J., Zhang J., Wang H.., Wang H., Anti‐Corrosion for Reversible Zinc Anode via a Hydrophobic Interface in Aqueous Zinc Batteries. *Adv. Energy Mater.* **2022**, *12*, 2103557.

[42] Geng L., Meng J., Wang X., Han C., Han K., Xiao Z., Huang M., Xu P., Zhang L., Zhou L.., Mai L., Eutectic Electrolyte with Unique Solvation Structure for High‐Performance Zinc‐Ion Batteries. *Angew. Chem. Int. Ed.* **2022**, *61*, e202206717.

[43] Nie X., Miao L., Yuan W., Ma G., Di S., Wang Y., Shen S.., Zhang N., Cholinium Cations Enable Highly Compact and Dendrite‐Free Zn Metal Anodes in Aqueous Electrolytes. *Adv. Funct. Mater.* **2022**, *32*, 2203905.

[44] Xie D., Wang Z. W., Gu Z. Y., Diao W. Y., Tao F. Y., Liu C., Sun H. Z., Wu X. L., Wang J. W.., Zhang J. P., Polymeric Molecular Design Towards Horizontal Zn Electrodeposits at Constrained 2D Zn^{2+} Diffusion: Dendrite‐Free Zn Anode for Long‐Life and High‐Rate Aqueous Zinc Metal Battery. *Adv. Funct. Mater.* **2022**, *32*, 2204066.

[45] Liu M., Cai J., Xu J., Qi K., Wu Q., Ao H., Zou T., Fu S., Wang S.., Zhu Y., Crystal Plane Reconstruction and Thin Protective Coatings Formation for Superior Stable Zn Anodes Cycling 1300 h. *Small.* **2022**, *18*, 2201443.

[46] Tao H., Hou Z., Zhang L., Yang X.., Fan L.-Z., Manipulating alloying reaction to achieve the stable and dendrite-free zinc metal anodes. *Chem. Eng. J.* **2022**, *450*.

[47] Li G., Wang X., Lv S., Wang J., Dong X.., Liu D., Long-life and low-polarization Zn metal anodes enabled by a covalent triazine framework coating. *Chem. Eng. J.* **2022**, *450*.

[48] Xu J., Lv W., Yang W., Jin Y., Jin Q., Sun B., Zhang Z., Wang T., Zheng L., Shi X., Sun B.., Wang G., In Situ Construction of Protective Films on Zn Metal Anodes via Natural Protein Additives Enabling High-Performance Zinc Ion Batteries. *ACS nano.* **2022**, *16*, 11392–11404.

[49] Wang M., Wu X., Yang D., Zhao H., He L., Su J., Zhang X., Yin X., Zhao K., Wang Y.., Wei Y., A colloidal aqueous electrolyte modulated by oleic acid for durable zinc metal anode. *Chem. Eng. J.* **2023**, *451*, 138589.

[50] Liu J., Song W., Wang Y., Wang S., Zhang T., Cao Y., Zhang S., Xu C., Shi Y., Niu J.., Wang F., A polyamino acid with zincophilic chains enabling high-performance Zn anodes. *J. Mater. Chem. A.* **2022**, *10*, 20779-20786.

[51] Wang F., Lu H., Zhu H., Wang L., Chen Z., Yang C.., Yang Q.-H., Mitigating the interfacial concentration gradient by negatively charged quantum dots toward dendrite-free Zn anodes. *Energy Stor. Mater.* **2023**, *58*, 215-221.

[52] Wang J., Qiu H., Zhang Q., Ge X., Zhao J., Wang J., Ma Y., Fan C., Wang X., Chen Z., Li G.., Cui G., Eutectic electrolytes with leveling effects achieving high depth-of-discharge of rechargeable zinc batteries. *Energy Stor. Mater.* **2023**, *58*, 9-19.

[53] Zhang J., Huang W., Li L., Chang C., Yang K., Gao L.., Pu X., Nonepitaxial electrodeposition of (002)-textured Zn anode on textureless substrates for dendrite-free and hydrogen evolution-suppressed Zn batteries. *Adv. Mater.* **2023**, *35*, e2300073.

[54] Shen Z., Mao J., Yu G., Zhang W., Mao S., Zhong W., Cheng H., Guo J., Zhang J.., Lu Y., Electrocrystallization Regulation Enabled Stacked Hexagonal Platelet Growth toward Highly Reversible Zinc Anodes. *Angew. Chem. Int. Ed.* **2023**, *62*, e202218452.

[55] Yuan W., Nie X., Ma G., Liu M., Wang Y., Shen S.., Zhang N., Realizing Textured Zinc Metal Anodes through Regulating Electrodeposition Current for Aqueous Zinc Batteries. *Angew. Chem. Int. Ed.* **2023**, *62*, e202218386.

[56] Wang H., Ye W., Yin B., Wang K., Riaz M. S., Xie B. B., Zhong Y.., Hu Y., Modulating Cation Migration and Deposition with Xylitol Additive and Oriented Reconstruction of Hydrogen Bonds for Stable Zinc Anodes. *Angew. Chem. Int. Ed.* **2023**, *62*, e202218872.

[57] Lu K., Chen C., Wu Y., Liu C., Song J., Jing H., Zhao P., Liu B., Xia M., Hao Q.., Lei W., Versatile 1, 3-dimethyl-2-imidazolidinone electrolyte additive: Enables extremely long life zinc metal batteries with different substrates. *Chem. Eng. J.* **2023**, *457*, 141287.

[58] Feng X., Li P., Yin J., Gan Z., Gao Y., Li M., Cheng Y., Xu X., Su Y.., Ding S., Enabling Highly Reversible Zn Anode by Multifunctional Synergistic Effects of Hybrid Solute Additives. *ACS Energy Lett.* **2023**, *8*, 1192-1200.

[59] Zhu Z., Jin H., Xie K., Dai S., Luo Y., Qi B., Wang Z., Zhuang X., Liu K., Hu B., Huang L.., Zhou J., Molecular-Level Zn-Ion Transfer Pump Specifically Functioning on (002) Facets Enables Durable Zn Anodes. *Small.* **2022**, *18*, e2204713.

[60] Fu H., Xiong L., Han W., Wang M., Kim Y. J., Li X., Yang W.., Liu G., Highly active crystal planes-oriented texture for reversible high-performance Zn metal batteries. *Energy Stor. Mater.* **2022**, *51*, 550-558.

[61] Zhang X., Li J., Qi K., Yang Y., Liu D., Wang T., Liang S., Lu B., Zhu Y.., Zhou J., An Ion-Sieving Janus Separator toward Planar Electrodeposition for Deeply Rechargeable Zn-Metal Anodes. *Adv. Mater.* **2022**, *34*, e2205175.

[62] Qin H., Kuang W., Hu N., Zhong X., Huang D., Shen F., Wei Z., Huang Y., Xu J.., He H., Building Metal‐Molecule Interface towards Stable and Reversible Zn Metal Anodes for

Aqueous Rechargeable Zinc Batteries. *Adv. Funct. Mater.* **2022**, *32*, 2206695.

[63] Li J., Lin Q., Zheng Z., Cao L., Lv W.., Chen Y., How Is Cycle Life of Three-Dimensional Zinc Metal Anodes with Carbon Fiber Backbones Affected by Depth of Discharge and Current Density in Zinc–Ion Batteries? *ACS Appl. Mater. Interfaces* **2022**, *14*, 12323-12330.

[64] Cheng Z., Wang K., Fu J., Mo F., Lu P., Gao J., Ho D., Li B.., Hu H., Texture Exposure of Unconventional (101)Zn Facet: Enabling Dendrite‐Free Zn Deposition on Metallic Zinc Anodes. *Adv. Energy Mater.* **2024**.

[65] Liu Y., Xie B., Hu Q., Zhao R., Zheng Q., Huang X., Deng S., Huo Y., Zhao J., Xu B.., Lin D., Regulating the helmholtz plane by trace polarity additive for long-life Zn ion batteries. *Energy Stor. Mater.* **2024**, *66*, 103202.

[66] Zhao Y., Guo S., Chen M., Lu B., Zhang X., Liang S.., Zhou J., Tailoring grain boundary stability of zinc-titanium alloy for long-lasting aqueous zinc batteries. *Nat. Commun.* **2023**, *14*, 7080.